Experimental Investigation of Mechanical Properties of 3D-Printing Built Composite Material

Yi-Tang Kao, Trace Dressen, Dong Sung (Danny) Kim,
Sima Ahmadizadyekta, Bruce L. Tai *

*Department of Mechanical Engineering, Texas A&M University, College Station, 77843

Keywords: 3D printing, additive manufacturing, composite materials
REVIEWED

Abstract

This paper studies the mechanical behaviors of a new composite material manufactured by 3D printing and polymer impregnation techniques. This composite uses 3D-printed plaster with an open-cellular structure as a frame to encapsulate the silicone resin (PDMS) to form a solid body. Because of the vastly different characteristics of the materials that make it up, the composite could have a wide variety of mechanical behaviors. In this study, design of experiment was performed with four-point bending tests using different composition ratios and sizes of open cells to determine the mechanical properties of the composite. These properties include maximum flexural stress (σ_{max}), flexural secant modulus of elasticity (E_f), and toughness indices (I_5 and I_{20}). The experimental results show that both E_f and σ_{max} are proportional to the plaster content and the unit cell size, while I_{20} had an opposite trend. The E_f ranged from 20 to 280 MPa, and σ_{max} ranged from 0.3 to 1.2 MPa for a 25%-75% plaster content and 3.25-6.5 mm cell size. Statistical analysis further confirmed the differences between these cases. This paper has demonstrated the capability of this composite to exert different mechanical properties for functional applications.

Introduction

Additive manufacturing (sometimes referred to as "3D printing") is an emerging technology used to build three-dimensional structures based on layer-by-layer deposition [1]. The main advantages of this technology include the ability to create almost any complex and light structure [2], minimize the material used, and decrease the cost for manufacturing small amounts of parts. The revolution of 3D-printing technology is undeniable, and it is evolving toward producing functional materials for practical use, such as composites. Recently, some 3D printers have been built with the ability to print multiple materials at the same time. For example, a commercially available printer, ProJet 5500X (3D Systems, Rock Hill, SC), prints rigid plastic and rubber-like materials with different material transparency and colors. The Objet Connex500 (Stratasys, Edina, MN) can print photopolymer, digital ABS, and rubber-like materials with varying material transparency and colors. Thus far, the amount of the available printing materials is still limited, and there is no significant difference in the properties of the materials used to create composites.

Other research on additively fabricating composites also continues. Laminated object manufacturing builds laminated fiber composites such as ceramic matrix composites (SiC/SiC) and polymer matrix composites (glass/epoxy) [3,4]. A selective laser sintering/melting technique has also been used for manufacturing various composite materials, such as metal-metal, polymer-

metal, polymer-ceramic, and metal-ceramic composites [5]. H. Kyogoku et al. reported the applicability of laser melting for manufacturing Ti-Ni shape memory alloys [6]. D.D. Gu et al. studied mechanisms in laser melting for a Cu–CuSn–CuP mixed powder [7]. K.K.B. Hon and T.J. Gill presented an experimental study in selective laser sintering for Silicon Carbide/Polyamide matrix composites [8]. H.S. Chung and Suman Das investigated selective laser sintering for functionally graded materials, which are composites of Nylon-11 and different volumes of glass beads [9]. These studies provide a variety of options in material preparation to strengthen 3D-printed parts. However, such composite printing focuses on the material itself and does not have the flexibility to create a part with structurally anisotropic properties for directional or localized strengthening. This paper, therefore, presents a new concept for the future application of 3D printing technology that can construct a composite of not only multiple materials but also with selected structural strength. The proposed composite consists of two or more vastly different materials and thus possesses a broader range of mechanical properties (from brittle to ductile) that could be tailored by manufacturers. Furthermore, different geometrical arrangements of these two phases can create different directional strengths. This concept is similar to the reinforced concrete used in construction with concrete as a rigid base and rebar as a tough addition. Owing to the flexibility of 3D printing, the desired structure design can be easily fabricated. In this study, a conceptual prototype was made with a powder-bed printer for the brittle phase and then combined with a silicone material as the ductile phase. The objective is to experimentally measure the changes in mechanical properties of the built composite and determine the effects of composition and structure.

In this paper, Section 2 will detail the material and methods used in the experimentation, followed by the results and discussion in Section 3. Section 4 presents the major conclusions and future works of this topic.

Materials and Methods

Sample preparation

A four-point bending test was utilized to examine the material properties of the composites. The test sample was designed to be 128 mm × 13 mm × 6.5 mm based on an open-cellular unit cubic structure to accommodate the silicone material, as shown in Fig. 1. The porosity of the part is determined by a unit cubic cell with a specific void-to-body ratio as shown in Fig.1 (a). The unit cells are assembled to form the part as shown in Fig. 1 (b) and (c). The complementary percentage of this ratio is defined as the composition ratio. A different structure could be made with an identical composition ratio. For example, the sample in Fig. 1 (b) is made of unit cells 6.5 mm in outer length with a composition ratio of 50%, compared to the sample in Fig. 1 (c) with 3.25 mm long cells and the same composition ratio.

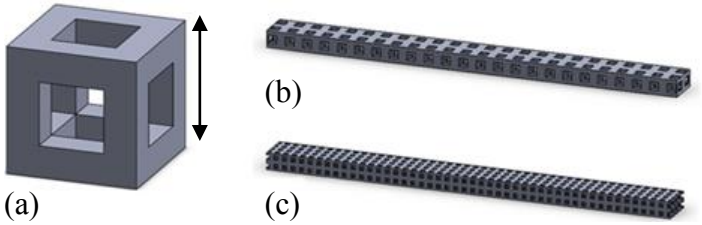

Figure 1 Sample design: (a) a unit cubic cell, (b) the frames based on the unit cubic cells of 6.5 mm and (c) 3.25 mm.

ProJet 160 (3D Systems, Rock Hill, SC), a commercial powder-bed 3D printer, was selected in this study for creating the frames. The powder material for this printer was VisiJet PXL, which contained 80 to 90% calcium sulfate hemihydrate (also known as plaster). A low elastic modulus silicone resin (PDMS), Sylgard 184 (Dow Corning, Midland, MI), was used along with the plaster frame to build the composite material. A mold, as shown in Fig. 2, was built using three separate aluminum plates to hold and cure the composite.

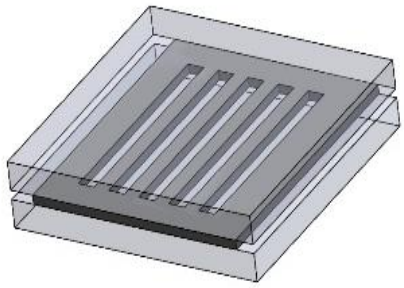

Figure 2 The mold for fabricating the composite samples

The steps for fabricating composite samples are summarized as follows: First, the silicone resin was fully mixed with hardener (Sylgard 184 curing agent, Dow Corning) in a disposable plastic cup with a 10:1 ratio according to the material datasheet. Then, the mixed silicone resin was completely degassed and poured into the mold. The pure plaster frames were baked for 10 minutes at 80˚C in an air oven and then placed into the slot of the mold filled with the silicone resin. The uncured composites were degassed again to remove any remaining air bubbles. Finally, the whole mold was placed into the air oven to bake at 80˚C for 2.5 hours to fully cure the composite. Samples were then removed from the mold for testing.

Experimental setup and design

The experimental setup for the four-point bending test is shown in Fig. 3, consisting of a linear actuator and a force transducer. The linear actuator (L70, Moog Animatics, Milpitas, CA) was driven by a servo-motor for a precise position and accurate feed rate control. Due to an anticipated small force, a high-sensitivity and high-response frequency force dynamometer (Model 9272, Kistler, Winterthur, Switzerland) was used to capture the force data. An amplifier, a shielded connector block, and a data acquisition device (PCIe-6321, National Instruments, Austin, TX) were used for data collection, along with LabVIEW as a data recorder.

As shown in Fig. 3, the loading nose and the loading support both had a cylindrical contact surface with a 5 mm radius. The support span was 128 mm and the loading span was 64 mm, in accordance with the ASTM-D7264 standard [10]. The feed rate of the loading support was 1.27 mm/min (0.05 inches/min); the maximum displacement of the loading noses was 50.8 mm (2 inches), which was the hardware limit with this setup.

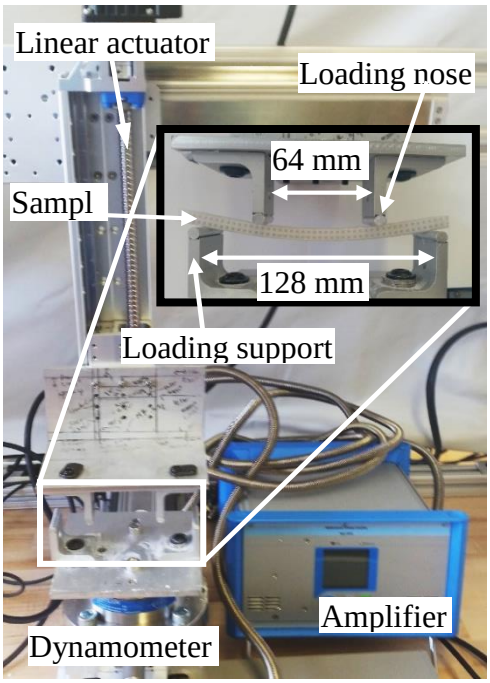

Figure 3 Experimental setup configured for the four-point bending test

In design of experiment, four different composition ratios were made for testing, including 25%, 50%, 75%, and 100%. The results with these different composition ratios were compared to the results of pure silicone and pure plaster samples to quantify the strengthening effects of the composites. In addition, for every composition ratio of a composite, there were two different structures: 6.5 mm and 3.25 mm long unit cells. These different structures were used to determine how the structures affected the material properties beyond the composition ratio. In total, there were six cases and one pure plaster case. Samples are shown in Fig. 4, where large and small unit cells are denoted by L and S, respectively. Each sample had five replicas for the bending test.

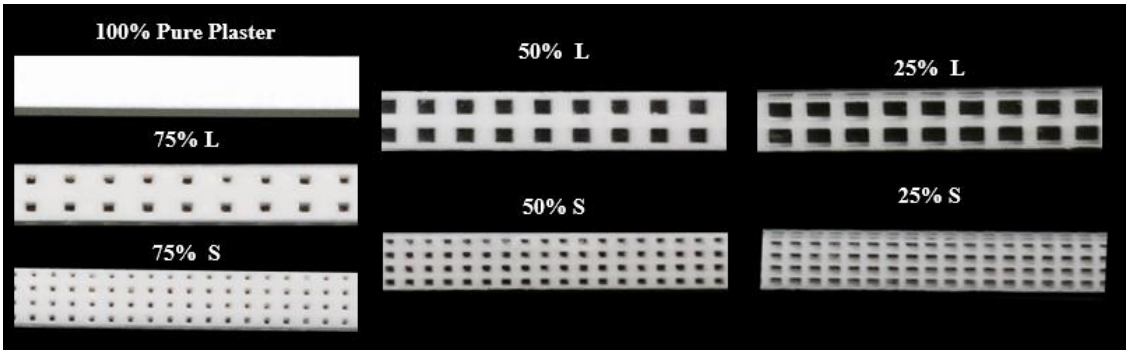

Figure 4 Completed composite samples with four composition ratios (25%, 50%, 75% and 100%) and two types of unit cells (L and S)

Three mechanical properties were obtained from the four-point bending test, including maximum flexural stress (σ_{max}), flexural secant modulus of elasticity (E_f), and toughness indices (I_5 and I_{20}). Following the ASTM standard, σ_{max} is calculated by Eq. (1)

$$\sigma_{\max} = \frac{3PL}{4bh^2} \tag{1}$$

where P is the maximum force applied, b is the width of sample (13mm), h is the height of sample (6.5 mm), and L is the support span (128 mm) of the four point bending setup. The E_f is calculated by Eq. (2)

$$E_f = \frac{0.17L^3m}{bh^3} \tag{2}$$

where L, b, and h are the same as those in Eq. (1), and m is the slope of the force-deflection curve within the elastic (linear) region. The toughness is represented by toughness indices (I_5 and I_{20}) described in ASTM 1018 [11]. Since the four-point bending samples do not have a notch at the mid-span, the flexural toughness could not be obtained. Instead, the toughness indices, based on the force-deflection curve, are described by

$$I_5 = \frac{A(3\delta_1)}{A(\delta_1)}, I_{20} = \frac{A(10.5\delta_1)}{A(\delta_1)} \tag{3}$$

where A is the area under the curve at a certain deflection and δ_1 is the first cracking point. The first cracking point is defined by the transition from a linear region into a non-linear region, equivalent to the yielding point in a tensile test.

Experimental Results

Both qualitative and quantitative comparisons are conducted in this section. Fig. 5 shows the average force-deflection curves of the composite materials to illustrate the differences in their mechanical behaviors. Each curve representing a composite sample is calculated based on the test results of five replicas. The pure plaster sample is not shown in the figure as it has a maximum average force of 36.5 N, with a rupture deflection of 2.9 mm, both of which are vastly different than the composite samples. This indicates that the pure plaster is relatively brittle. As shown in Fig. 5, 75% plaster samples (both L and S) break before the maximum deflection of 50.8 mm since the plaster structure dominates the mechanical behavior. However, in the cases of the 50% and 25% plaster samples, no rupture occurs prior to the maximum deflection.

For the elastic performance, all the samples display a nearly elastic behavior when the deflections of the midpoints are lower than 3.5 mm, regardless of the composition ratios and structures. This is because the elastic region is, again, dominated by the plaster structure. Moreover, this is also the reason for crack occurrences at the same strain (midpoint deflection). In general, the slopes of the force-deflection curves significantly decrease once the deflections exceed 3.5 mm. At this point, the plaster frame of a sample cracks and the silicone portion begins to act as rebar to hold the structure together and prevent crack propagation. Therefore, 3.5 mm is defined as the first cracking point (δ_1) for the following toughness indices calculation. After the δ_1, the force either increases slowly or remains at a nearly constant level. This is because of the exceptional ductility of the silicone resin.

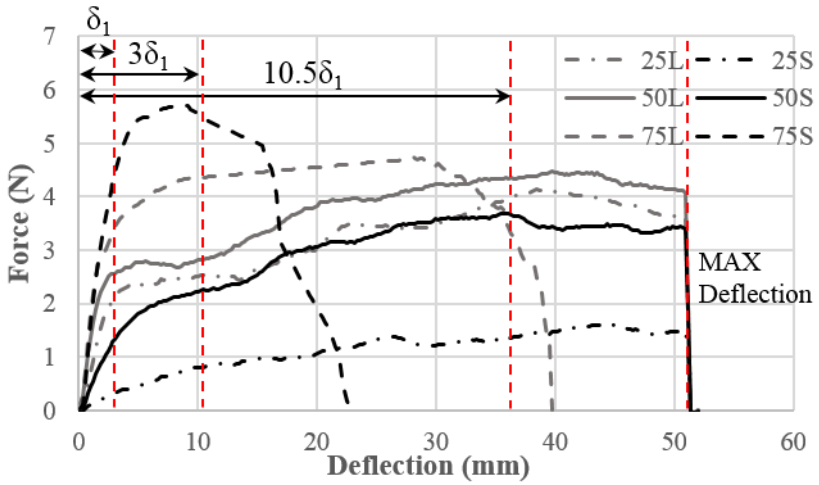

Figure 5 Averaged force-deflection curves for the composite samples.

Based on the averaged data, toughness indices of the composite samples were calculated and are shown in Fig. 6. All the samples have similar I_5. This indicates that, immediately after the δ_1, the force-deflection curves change in a similar trend for all the samples despite different magnitudes. In contrast, the results of the I_{20} are quite different for all the samples. Samples with a lower amount of the plaster (i.e., lower composition ratio) possess higher I_{20}, meaning the silicone resin contributes to the toughness more at a larger deflection. In addition to the composition ratio, the sample structure (i.e., unit cell size) plays an important role in the toughness index I_{20}. The I_{20} of large-cell samples with 25% and 50% composition ratios are smaller than those with small cells. However, the 75% samples display an opposite phenomenon.

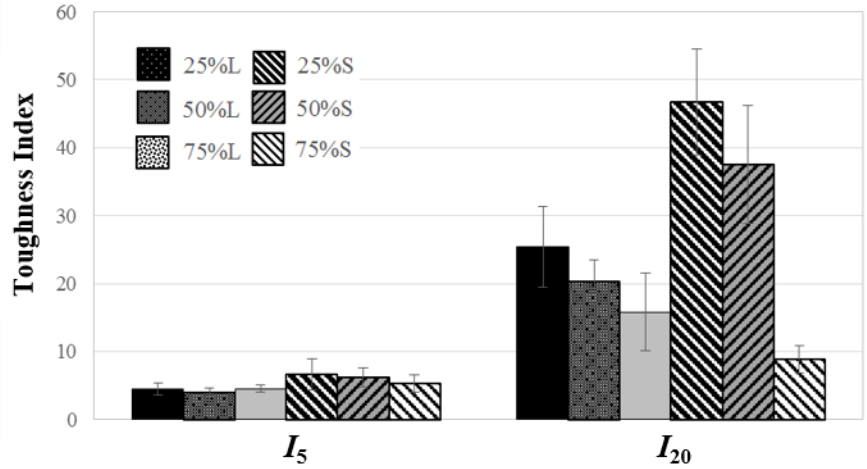

Figure 6 Toughness indices of plaster-silicone composite samples.

Fig. 7 shows the statistical results of flexural secant moduli of elasticity (E_f) for all composite samples. The slope was fitted in the first 0.04 mm of the force-deflection curve for each sample to find E_f. Pure plaster and pure silicone cases are not shown in the figure due to their relatively extreme properties. The pure plaster solid sample has an E_f up to 1611 MPa, while the E_f of a pure silicone resin is nearly zero because it could not resist any bending moment. Results

in Fig. 7 suggest an increasing E_f with the composition ratio. The E_f is dominated by the amount of plaster in the structure because it possesses a much higher stiffness than silicone resin. Statistical analysis using a t-test also confirms a significant difference in E_f when the composition ratio increases. On the other hand, for a given composition ratio, samples with a larger unit cell structure tend to have a higher E_f. Statistically, there is a significant difference between small- and large-cell samples, excepting the case of 75% due to the variations.

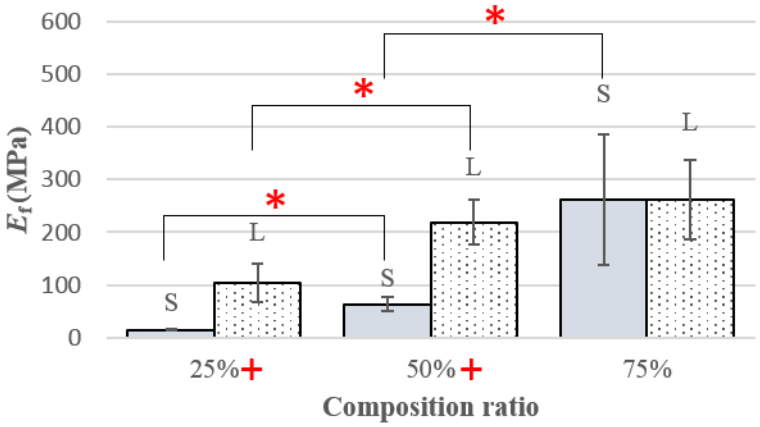

Figure 7 Flexural secant moduli of elasticity (E_f) for plaster-silicone composite samples.
* represents a statistical significance ($p < 0.05$) between different composition ratios;
+ means a statistical difference between small and large cell samples.

Fig. 8 shows the maximum stress (σ_{max}) for all the samples. The σ_{max} of the pure plaster samples was 6.15 MPa on average, and that of the pure silicone was not available due to a nearly-zero stiffness in the bending test. For the composite materials, σ_{max} increases with the composition ratio because the plaster material is the major source of the strength. Statistical results revealed that the samples with the same unit cell but different composition ratios could be different in σ_{max}, particularly for small-cell samples. If comparing σ_{max} based on the sample structure, the samples with a larger unit cell have higher σ_{max} than those with small unit cells. This phenomenon is similar to the results of E_f in Fig. 7.

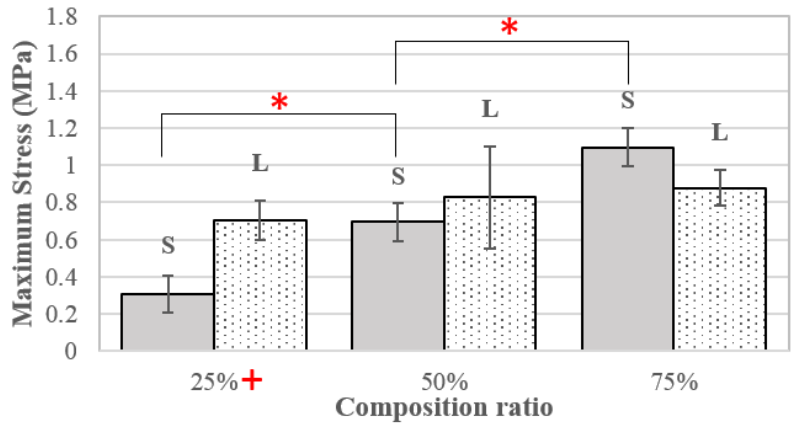

Figure 8 Maximum stress (σ_{max}) for plaster-silicone composite samples.
* represents a statistical significance ($p < 0.05$) between different composition ratios;
+ means a statistical difference between small and large cell samples.

Discussion

The results suggested that both composition ratio and structure can affect the mechanical properties of the plaster-silicone composites. Since the data was obtained via four-point bending tests, the flexural secant moduli of elasticity (E_f), maximum stress (σ_{max}), and toughness index (I_{20}) are largely dependent on the resistance against the moment. That is, a resultant bending stiffness (i.e., the production of elastic modulus and moment of inertia) plays an important role in the composite materials.

In regards to E_f (in Fig. 7), the samples with large and small unit cells are anticipated to have the same elasticity under a uniaxial tension; however, samples with a larger unit cell display higher moduli in a bending case due to a higher moment of inertia. The difference in the 75% case could be due to variations in the samples.

Similarly, in regards to σ_{max} (Fig. 8), structures with larger cells also possess higher σ_{max}. It is important to note that this stress is calculated based on a homogenous cross-section. Therefore, this stress does not mean an absolute higher stress on the outer surface of the structure. Instead, it is a result of a higher E_f under the same strain (deflection). Another possible reason is that a larger unit cell has a better structural integrity than a smaller unit cell. The powder printing material has a size of 10 to 100 μm in diameter. Thus, with a feature size in mm or sub-mm scales, the number of particles within each structural feature could be critical to its strength.

Having seen the differences in the mechanical properties of these samples, it would be of interest to see if there exists a model to predict these properties for design purposes. A typical model for composite materials is known as the rule of mixtures. This model gives the upper and lower bounds of a composite material with the reinforced fibers parallel or perpendicular to the stress flow, known as the iso-strain and iso-stress conditions. The equations are given by Eq. (4) and Eq. (5), respectively [12].

$$E_c = V_s E_s + V_p E_p \tag{4}$$

$$E_c = \frac{E_p E_s}{E_p V_s + E_s V_p} \tag{5}$$

where, in our case, E_p and E_s are the elastic moduli of plaster and silicone resin, and V_p and V_s are their volume fractions, respectively. The E_s is set as 1.78 MPa, adopted from the literature [12], since it is too low to be measured in the four-point bending test. The E_P in this study is 1.61 GPa. Fig. 9 shows the upper and lower bounds of this type of composite material. As expected, both large and small cell samples fall within the boundaries. An empirical rule of mixture can be established when a sufficient amount of data points are added to the plot. In addition, it can also be found that the small-cell samples are closer to the average of the upper and lower bounds, which is an isotropic mixing condition. This fact verifies that small-cell samples act more like a homogeneously mixed material due to the fine grid inside the material.

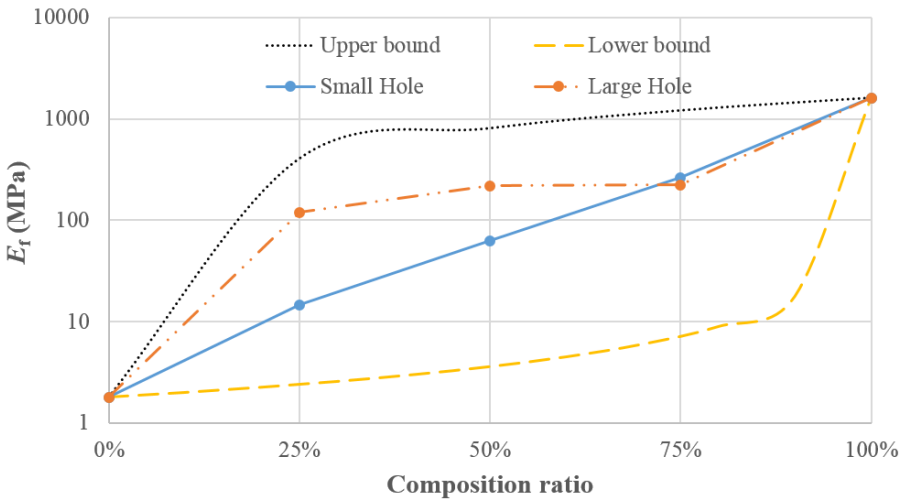

Figure 8 The upper and lower bounds of the composite samples based on the rule of mixtures.

Although the current data and statistical analyses have suggested the basic trends of properties change in accordance to the composition ratio and structure, there were still limitations in this study: first, the variations were large, which resulted in an insufficient statistical power to distinguish samples; second, more levels in both structure and composition ratio in the design of experiments are needed to lead to more solid conclusions; third, only one type of silicon resin was used, so it is unknown if the results are applicable to general cases.

Conclusions

This paper presented a new concept of composite material built using 3D printed part as the brittle material and durable silicone material as the ductile material, aiming to create a reinforced structure for functional applications. Prototype samples made of 3D printed plaster and silicone resin were fabricated with various composition ratios and structures for the four-point bending test in order to obtain the mechanical properties. Based on the data, the major findings in this paper are:

- Given the extreme properties of brittle and ductile materials, a composite with a wide variety of mechanical properties can be created.
- The brittle material dominates the strength and elastic modulus of the material, while the ductile material controls the toughness. A balance between these two materials could maximize the material's functionality.
- The mechanical properties of the composites are determined by both the composition ratios of these two materials and the structural configuration (i.e., unit cell size).
- The composites composed of small unit cells tend to behave as a homogenous mixture of two materials, but a better strength and stiffness are often provided by larger unit cells, particularly in bending.
- The rule of mixtures could be applicable to this type of composite.

The future works of this study include testing different combinations of the materials to generalize the rule of mixtures model, investigating the failure mechanism of the composites, and exploring a hybrid manufacturing process to build the composites at a time without manual operations in molding.

Acknowledgments

This research is supported by the National Science Foundation grant #1522877. The authors would also like to acknowledge the material supports from Dow Corning.

References

1. Hung, K.C., Tseng, C.S., and Hsu, S.H., *Synthesis and 3D printing of biodegradable polyurethane elastomer by a water-based process for cartilage tissue engineering applications.* Adv Healthc Mater, 2014. **3**(10): p. 1578-87.
2. Wong, K.V. and Hernandez, A., *A Review of Additive Manufacturing.* ISRN Mechanical Engineering, 2012. **2012**: p. 1-10.
3. Kruth, J.P., Leu, M.C., and Nakagawa, T., *Progress in Additive Manufacturing and Rapid Prototyping.* CIRP Annals - Manufacturing Technology, 1998. **47**(2): p. 525-540.
4. Donald A. Klosterman, Richard P. Chartoff, Brian Priore, Nora Osborne, George Graves, Allan Lightman, Sung S. Pak, and Weaver, J., *Structural Composites via Laminated Object Manufacturing (LOM)*, in *Solid Freeform Fabrication Symposium*. 1996. p. 105-116.
5. Kruth, J.P., Levy, G., Klocke, F., and Childs, T.H.C., *Consolidation phenomena in laser and powder-bed based layered manufacturing.* CIRP Annals - Manufacturing Technology, 2007. **56**(2): p. 730-759.
6. Kyogoku, H., Ramos, J.A., and Bourell, D.L., *Laser Melting of Ti-Ni Shape Memory Alloy*, in *Solid Freeform Fabrication Symposium*. 2002: Austin. p. 668-675.
7. Gu, D., Shen, Y., Fang, S., and Xiao, J., *Metallurgical mechanisms in direct laser sintering of Cu–CuSn–CuP mixed powder.* Journal of Alloys and Compounds, 2007. **438**(1-2): p. 184-189.
8. Hon, K.K.B. and Gill, T.J., *Selective Laser Sintering of SiC/Polyamide Composites.* CIRP Annals - Manufacturing Technology, 2003. **52**(1): p. 173-176.
9. Chung, H. and Das, S., *Processing and properties of glass bead particulate-filled functionally graded Nylon-11 composites produced by selective laser sintering.* Materials Science and Engineering: A, 2006. **437**(2): p. 226-234.
10. ASTM, *Standard Test Method for Flexural Properties of Polymer Matrix Composite Materials*.
11. ASTM, *Standard Test Method for Flexural Toughness and First-Crack Strength of Fiber-Reinforced Concrete*.
12. Kim, H.S., *On the rule of mixtures for the hardness of particle reinforced composites.* Materials Science and Engineering: A, 2000. **289**(1-2): p. 30-33.